
Investigating Generalization Behaviours of Generative Flow Networks

Lazar Atanackovic^{1,2†} Emmanuel Bengio³

Abstract

Generative Flow Networks (GFlowNets, GFNs) are a generative framework for learning unnormalized probability mass functions over discrete spaces. Since their inception, GFlowNets have proven to be useful for learning generative models in applications where the majority of the discrete space is unvisited during training. This has inspired some to hypothesize that GFlowNets, when paired with deep neural networks (DNNs), have favourable *generalization* properties. In this work, we empirically verify some of the hypothesized *mechanisms* of generalization of GFlowNets. In particular, we find that the functions that GFlowNets learn to approximate have an implicit underlying structure which facilitate generalization. We also find that GFlowNets are sensitive to being trained offline and off-policy; however, the reward implicitly learned by GFlowNets is robust to changes in the training distribution.

1. Introduction

Generative Flow Networks (GFlowNets, or GFNs) have emerged as a generative modelling framework for learning unnormalized probability mass functions of discrete objects such as graphs, sequences, or sets (Bengio et al., 2021; 2023). They have especially shown promise for a wide range of problems and applications where optimization is conducted over very large combinatorial spaces. To name a few, discrete probabilistic modelling (Zhang et al., 2022), molecular discovery (Bengio et al., 2021; Jain et al., 2023), biological sequence design (Jain et al., 2022), and causal discovery (Deleu et al., 2022; 2023; Atanackovic et al., 2023) are areas where the discrete spaces may be intractably large. In these applications, the model will realistically only visit a small fraction of the overall state space. Therefore, under-

standing how well GFlowNets model and assign probability mass to the unvisited areas of the state space is a critical step. This is fundamentally a question of *generalization*.

Generalization of deep neural networks (DNNs) in supervised learning and deep learning has been extensively studied (Leshno et al., 1993; Pascanu et al., 2013; Zhang et al., 2017; 2021; Kawaguchi et al., 2017). Although it is still not entirely understood, many mechanisms and intuitive notions for generalization have emerged as the favored schools of thought (Arpit et al., 2017) and inspire this work. Due to their close relationship with GFlowNets, works studying generalization in Reinforcement Learning also inspire this work (Zhang et al., 2018; Packer et al., 2018; Cobbe et al., 2019; Bengio et al., 2020).

It has been hypothesized that GFlowNets work well because they synergistically leverage the generalization potential of DNNs to assign probability mass in unvisited areas of the state space (Bengio et al., 2021), and while the works of Nica et al. (2022) and Shen et al. (2023) probe at this question, they only do so superficially. Indeed, questions regarding the *mechanisms* of generalization in GFlowNets have yet to be systematically investigated and wholly understood. With this comes a natural question – *how well* do GFlowNets generalize to *unvisited* areas of the state space? Thus, unravelling some intuitive notions on *why* and *how* GFlowNets generalize forms the basis of this work.

We center our investigation around three primary hypotheses for generalization in GFlowNets:

1. GFlowNets generalize well when their **self induced training distributions are nice**, i.e. sampling on-policy from $P_F(s'|s; \theta)$, or proportionally to $R(s)$, is ideal.
2. GFlowNets generalize well because the **objects they are learning have structure**; $P_F(s'|s)$ and $F(s)$ are not “arbitrary” functions.
3. The difficulty for GFlowNets to generalize is modulated more by the **complexity of the reward** (as perceived by a DNN) than the properties of the distribution induced by the reward.

To investigate these hypotheses, we devise an empirical investigation to *disentangle* some of the *mechanisms* that lead to generalization when training GFlowNets. We structure

[†]Work was done during an internship at Valence Labs.
¹University of Toronto ²Vector Institute ³Valence Labs. Correspondence to: Lazar Atanackovic <l.atanackovic@mail.utoronto.ca>, Emmanuel Bengio <emmanuel.bengio@valencelabs.com>.

our study on the basis of making simplifying assumptions such that we reduce the complexities/moving parts of training GFlowNets. These “moving parts” may otherwise act as confounding variables when investigating mechanisms. This approach helps us isolate specific factors of variation which may play a role in *why* GFlowNets generalize.

We describe the details of our experimental setup in §3, and to this end, construct comprehensive benchmark tasks with well defined and tractably computable $p(x; \theta)$, $\forall x \in \mathcal{X}$, presented in §2.

We note that our proposed empirical study helps us disentangle some of the mechanisms of generalization in GFlowNets, but does not necessarily determine the true underlying causal order of these mechanisms. Nonetheless, we believe this work can pave a road-map for how to approach testing generalization of GFlowNets and view this as a key step towards understanding important properties for this class of algorithms.

Our main contributions are summarized as follows:

- We propose a set of benchmark graph generation tasks of varying difficulty, useful for evaluating GFlowNets’ generalization performance.
- We reify and validate some hypothesized characteristics of GFlowNet generalization behaviour over discrete spaces. We accomplish this empirically using benchmark tasks.
- We identify and present a set of observations and empirical findings that form a basis towards disentangling some of the *mechanisms* for generalization of GFlowNets.

For the sake of clarity, we define some terms that we want to make as least ambiguous as possible in §A.

1.1. Generative Flow Networks

Generative Flow Networks (GFlowNets, GFNs) are a generative modeling framework used to learn to sample from an unnormalized probability distribution. We will refer to this unnormalized function as a positive *reward*, $R(s) > 0$. Introduced in the discrete setting (Bengio et al., 2021), but since then extended to continuous settings (Lahlou et al., 2023), GFlowNets work by learning a sequential, constructive sampling policy. This policy, P_F , is used to sample trajectories $\tau = (s_0, \dots, s_t)$ where states $s \in \mathcal{S}$ are partially constructed objects, making the state space a pointed directed acyclic graph (DAG) $\mathcal{G} = (\mathcal{S}, \mathcal{A})$ where $(s \rightarrow s') \in \mathcal{A} \subset \mathcal{S} \times \mathcal{S}$ is a valid constructive step. There is a unique initial state s_0 .

While they can be expressed in multiple equivalent ways, we will think of GFlowNets in this work through three main

objects: the flow of a state $F(s) > 0$, and the forward and backward policies, $P_F(s'|s)$ and $P_B(s|s')$. In a perfect GFlowNet, these functions are such that for any valid partial trajectory (s_n, \dots, s_m) :

$$F(s_n) \prod_{i=n}^{m-1} P_F(s_{i+1}|s_i) = F(s_m) \prod_{i=n}^{m-1} P_B(s_i|s_{i+1}) \quad (1)$$

where for terminal (leaf) states, $F(s) = R(s)$ by construction. If the above equation is satisfied, then starting at s_0 and sampling from P_F guarantees to reach a leaf state $s_t \equiv x$ with probability $p(x) \propto R(x)$, $x \in \mathcal{X}$. We use \mathcal{X} to denote the set of terminal (leaf) states. Note that it may be useful to think of P_F and P_B as representing fractions of flows going forward and backward through the (DAG) network. It may also be useful to think of the flow going through edges: $F(s \rightarrow s') = F(s)P_F(s'|s)$.

The so-called *balance condition* in (1) leads to a variety of learning objectives. In this work we primarily use the Sub-trajectory Balance (specifically SubTB(1)) introduced by Madan et al. (2022), which takes the above conditions, parameterizes the log flow and logits of policies, taking the squared error over all possible subtrajectories:

$$\mathcal{L}_{\text{SubTB}}(\tau) = \sum_{n < m \leq T} \left(\log \frac{F(s_n) \prod_{i=n}^{m-1} P_F(s_{i+1}|s_i)}{F(s_m) \prod_{i=n}^{m-1} P_B(s_i|s_{i+1})} \right)^2. \quad (2)$$

We note that trajectory balance (TB) is a special case of the above, where only $n = 0$ and $m = T$ are used. We also note from (1) that $P_F(s'|s) = P_B(s|s')F(s')/F(s) \propto F(s')$, and note that $F(s)$ is upper bounded (when P_B of all its descendant edges is 1) by the sum of the rewards of all its descendant leaves. For a complete overview of GFlowNets, we refer readers to Bengio et al. (2023).

2. A Benchmark Task for Investigating Generalization Behaviours of GFlowNets

As a first step, we present a novel benchmark environment built on a series of graph-based tasks. We use graphs as the foundation of the benchmark tasks as they are a natural choice for compositional discrete objects, and a wide range of combinatorial problems can be expressed as graph generation. Thus, we use a graph environment to define tasks of varying difficulty. This helps us standardize benchmarks for GFlowNets when investigating generalization and learning $p(x)$ since the environment can be held constant while the reward difficulty is varied. However, for completion, we also conduct experiments on two commonly used environments and tasks in GFlowNet literature: the **hypergrid** and **sequence** environments. In the following, we present our graph-based benchmark environment and the corresponding tasks considered in this work.

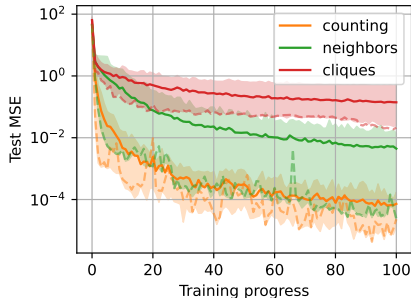


Figure 1. Training a GNN on 3 different tasks with models of varying capacity. Most of the variance comes from varying capacity. Dashed lines are for the highest capacity models.

2.1. A Small Graph Environment

We setup an environment with all possible graphs of size 7 and less, where the nodes can be one of two colors. This environment has a total of 72296 states, which allows us to compute the true distribution $p(x)$ and the learned $p(x; \theta)$ for $x \in \mathcal{X}$ relatively quickly (in the order of 10 seconds on a GPU; see §C.1.2). We denote the set of graphs/states as \mathcal{X} . We define a number of reward functions that induce a variety of challenges for models.

Reward complexity: We define three different reward functions, which we hope to be of varying difficulty. The hardest function, **cliques**, requires the model to identify subgraphs in the state which are 4-cliques of at least 3 nodes of the same color. The second function, **neighbors**, requires the model to verify whether nodes have an even number of neighbors of the opposite color. Finally, the third function, **counting**, simply requires the model to count the number of nodes of each color in the state. We fully define and show the distribution of $\log R(x)$ of the respective tasks in §C.1. We can observe that the distribution of $\log R(x)$ increases in complexity relative to the hardness of the underlying task.¹

We verify that our intuitive notion of hardness for these tasks translates to graph neural networks (GNNs). To do so we train standard graph attention networks (Veličković et al., 2017) with varying capacity to regress to the (log) reward functions. We use a 90%-10% train-test split, and show the resulting test error in Figure 1. We see that the ordering seems consistent with the difficulty of the task.

Structural generalization: The so-called *structural generalization hypothesis* posits that function approximators like deep neural networks (DNNs) capture regular patterns in the data (Arpit et al., 2017; Zhang et al., 2021), i.e. structure.

¹For example, the relative quantity of high reward states (“sparseness” of rewards over states) and the general distribution of $\log R(x)$ (“discontinuity” of reward distribution) are factors that can drive learning difficulty.

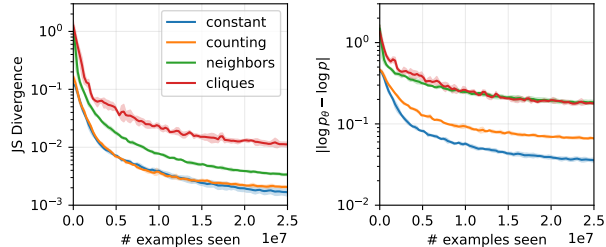


Figure 2. Training a GFlowNet (online and on-policy) on 4 different tasks. While ordering is mostly preserved, apparent difficulty depends on the choice of metric.

This enables models to make accurate predictions on similarly structured inputs not present in the training set. In our investigation, we reify this intuition by introducing a structured test set. We generate a test set randomly (with seeds of course) by picking states with at least 6 nodes (this choice is not arbitrary, see §C.1.3) and adding *all their descendants* to the test set. We do so iteratively until the test set is of the desired size. We include further details in §C.1.3. Generalizing to a “structured” test set this way poses a more challenging problem than simply selecting test samples i.i.d. from the data distribution (Tossou et al., 2023).

Metrics for Performance: We aim to evaluate how well GFlowNets model and learn the distribution $p(x)$ over all states $x \in \mathcal{X}$. To do this, we consider 2 distributional metrics: Jensen-Shannon (JS) divergence and mean absolute error (MAE) between $\log p(x)$ and the learned $\log p(x; \theta)$. We describe details for these metrics in §C.4. We also note that when generating graphs, properly taking into account isomorphic actions is essential to learning the right $p(x; \theta)$ (see Ma et al., 2023, for reference).

2.2. Difficulty of Tasks is Preserved When Training GFlowNets Online and On-policy

We now verify that training GFlowNets on our proposed graph environment and defined tasks yields the task ranking that we’d expect. We train GFlowNets online with SubTB(1) and a uniform P_B .

To lower bound the modeling complexity, we add a fourth reward, one where $R(x) = 1, \forall x \in \mathcal{X}$.² Note that for this specific experiment there are no states hidden from the model, i.e. no test set, since the model is able to sample from its policy and explore the entirety of the state space.

²Note that, hypothetically, this may be harder than other rewards. For a constant reward, the model has to learn to put *equal probability mass everywhere*, which means being able to model the entire state space. In contrast, more complex but “peakier” reward functions may be in some sense easier to “get right” if one cares more about modeling high-reward states, since there are presumably fewer of them.

We will start using a test set in §4.1. Here, we are only verifying the difficulty of the “usual” GFlowNet setup in the respective tasks.

Figure 2 shows interesting results. The ordering of tasks is more or less conserved, but depends on the metric we use to measure the discrepancy between $p(x)$ and $p(x; \theta)$. Using a constant reward indeed lower bounds other rewards, but not by much. This suggests that there is, unsurprisingly, inherent difficulty in modeling the dynamics of the environment.

We find that there are **two main axes** of difficulty with respect to the task (aside of course from the *scale* of the problem, which here is kept constant): (1) how *difficult* the reward is to model, and (2) how the reward is *distributed*. Hopefully, Figure 1 and Figure 2 are convincing evidence of (1). We will come back to (2) later in §4.2.

Readers are also hopefully now on board that this benchmark is sufficiently complex, and has interesting characteristics for empirical validation and hypothesis testing purposes. We also consider 2 non-graph environments, a **hypergrid** environment and **sequence** environment, with reasonably sized states spaces such that we can tractably compute $p(x; \theta)$ exactly. This allows us to investigate GFlowNet generalization behaviours in contexts other than graphs. Since the graph, hypergrid, and sequence environments are all discrete spaces, we expect general findings to be consistent across all tasks. We use tasks and reward functions used in prior GFlowNet work (Bengio et al., 2021; Malkin et al., 2022; Jain et al., 2023). We describe the setups and experimental details of these environments and tasks in §C.2.

3. A Method for Disentangling Generalization Mechanisms of GFlowNets

We consider 3 main experimental settings: (1) **distilling (regressing to) flow functions**, (2) **memorization gaps in GFlowNets**, and (3) **offline and off-policy training regimes**. Each experimental setup is built on a series of simplifying assumptions such that we can control for different moving parts and complexities that are present when training GFlowNets. We now present this experimental protocol, and then report and discuss our findings in §4.

3.1. Distilling (Regressing to) Flow Functions

Just as we can compute the distribution $p(x; \theta)$ over \mathcal{X} exactly in this environment, we also compute edge flows $F(s \rightarrow s')$ and $P_F(s'|s)$ exactly. We refer to these as the *true* flow and forward policies, in opposition to the approximated $F(s \rightarrow s'; \theta)$ and $P_F(s'|s; \theta)$. Note that we parameterize $F(s \rightarrow s'; \theta)$ and $P_F(s'|s; \theta)$ as mappings from $\mathcal{S} \rightarrow \mathbb{R}^{n(s)}$ where $n(s)$ is the number of children of s .

In this set of experiments, we train DNNs by regressing to the *true* flow³ $F(s \rightarrow s')$ and forward policy $P_F(s'|s)$. This removes the use of the GFlowNet training objective and the use of trajectories sampled from $P_F(s'|s; \theta)$ as the training data distribution, drastically simplifying the training procedure. As such, we basically control for any non-ideal factors introduced by the GFlowNet training objectives, for example, possible shortcomings due to temporal credit assignment (Malkin et al., 2022).

We can now train models to regress to $\log F(s \rightarrow s')$ or $\log P_F(s'|s)$. These are both vectors, so we regress to each value independently and minimize the mean squared error. Note that the true $P_F(s'|s) = \text{softmax}(\log F(s \rightarrow s'))$. Regressing to $\log F(s \rightarrow s')$ is the same general problem as regressing to $\log P_F(s'|s)$, but with one caveat. When learning $F(s \rightarrow s'; \theta)$, the model has to not only get the relative magnitudes of each logit right, but also the absolute magnitudes right. In contrast, when learning $P_F(s'|s; \theta)$, because of the normalization within the softmax, the model only has to get the relative magnitude of the logits right. Because of this, we expect that learning $P_F(s'|s)$ is easier, although learning flow magnitudes could help with generalization. For these experiments we set P_B to be the uniform policy to get unique F and P_F .

Using this setup we are able to assess how fundamentally difficult these flow functions are to learn. Furthermore, we can use our test set of unseen states. This allows us to assess generalization performance for learning $p(x)$ (which we are able to tractably compute) by directly computing distributional errors. Because of the use of a test set, this is in some sense more challenging than when training GFlowNets directly, i.e. online and on-policy, since standard training of GFlowNets allows the model to potentially explore the entire space and “see” the entire dataset.⁴

Overall, in this setting we can probe the question of “*do*” GFlowNets generalize when learning F or P_F and assess **Hypotheses 2 & 3**. In the following sub-section, we describe a second approach that can help us investigate some mechanistic intuitions of *why* flow functions might induce generalization in GFlowNets, probing the question of “*why do*” GFlowNets generalize.

3.2. Memorization Gaps in GFlowNets

We would like to probe our hypothesis on learning *true* flows and their contribution to generalization in GFlowNets. Here,

³In this sense, we are “distilling” the *true* flows into flow functions parameterized by a DNN.

⁴Readers may notice that in this task, because we’ve computed the regression targets F and P_F exactly using the entire state space, some information of the test set is leaking into the targets. Since the purpose of this experiment is to assess how hard these functions fundamentally are to learn, we knowingly allow the model to cheat.

Investigating Generalization Behaviours of Generative Flow Networks

Problem	Data Coupling	Reward (data)	Flow (environment)
		Structure	Structure
Regress R	$s \not\perp R(s)$	✓	✗
Regress R	$s \perp \tilde{R}(s)$	✗	✗
Regress P_F	$(s, s') \not\perp P_F(s' s)$	✓	✓
Regress P_F	$(s, s') \not\perp \tilde{P}_F(s' s)$	✗	✓
Regress P_F	$(s, s') \perp P_F^{\text{random}}$	✗	✗

Table 1. High level summary for the memorization gap experiments. Each row lists the setup of an individual experiment showing the corresponding data pair coupling and structure of learning problem.

we take on the perspective of Zhang et al. (2017; 2021) and consider generalization as the act of *not memorizing*. In other words, we can assess whether a model is generalizing or not by measuring the gap (in *training* performance) between training it on structured data and training on random unstructured data. We use this notion of *memorization gap* to try and reason about learning structured flows and their implications on generalization.

We devise an experiment inspired from Zhang et al. (2017; 2021), where we train supervised models by, similarly to the previous section, regressing to $R(s)$ and $P_F(s'|s)$, but with various degrees of “de-”structuring.

Consider simply learning to predict $R(s)$ with $R(s; \theta)$. If instead of regressing from s to $R(s)$ we shuffle the reward labels of each state s , we end up with new $(s, \tilde{R}(s))$ pairings. This induces independence between the data pairings, i.e. $s \perp \tilde{R}(s)$. Intuitively, training a DNN with $s \perp \tilde{R}(s)$ will force the DNN to memorize since we have removed any structured information that may exist in the problem. We compare the training curve gap between regressing to R and \tilde{R} .

Now consider regressing to $P_F(s'|s)$; there are two ways to destructure this function. Recall that $P_F(s'|s) \propto F(s')$, and that $F(s)$ is a function of the *reward* of all its descendants as well as of the *transition structure* of the state space (the ways to get to those descendants). Let $\mathcal{D}(s)$ be the set of descendants of s . By shuffling R into \tilde{R} , we thus remove the dependence between s and $\tilde{R}(s_d) \forall s_d \in \mathcal{D}(s)$, but keep the dependence between s and *how to get to* $\mathcal{D}(s)$. The second way to de-structure P_F is to simply regress to random logits, which we will denote P_F^{random} .

To recap, we train models on both the coupled and permuted or random data. We consider 5 overall experiments (see Table 1), regressing to: $R(s)$ using paired data, $R(s)$ using shuffled data, $P_F(s'|s)$ using paired data, $P_F(s'|s)$ using shuffled data, and $P_F(s'|s)$ using random logits P_F^{random} sampled (once before training) uniformly at random from a magnitude-preserving range. Table 1 summarizes the high level setup of each experiment and the corresponding

	$\mathbb{P}_{\mathcal{X}}$	Resemblance to Sampling x
Uniform	$\propto \mathcal{U}(x)$	i.i.d.
Log-rewards	$\propto R(x)$	from an ideal policy
Proxy for on-policy	$\propto p(x; \theta)$	\propto to $P_F(s' s; \theta)$
Absolute error	$\propto p(x; \theta) - p(x) $	\propto absolute loss
Squared log-error	$\propto (\log p(x; \theta) - \log p(x))^2$	\propto squared log-loss (e.g. SubTB(1))

Table 2. Details for different training distributions $\mathbb{P}_{\mathcal{X}}$ for offline and off-policy experiments.

data/flow structure of the problem.

Through this setup, we can assess the *memorization gap* that occurs when training models on the respective settings and tasks. In particular, removing the structure of the data but maintaining flow structure in the learning problem allows us to assess the contribution that learning *true* flows has on generalization (i.e. *not memorization*) when training GFlowNets. Following from **Hypothesis 2**, if state flows have interesting structure and learning structured flows reduces the degree of memorization, perhaps this structure inherently acts as a mechanism for generalization in GFlowNets.

3.3. Offline and Off-policy Training Regimes

Lastly, we would like to investigate the effects of deviating from the self-induced training distributions of GFlowNets on generalization. To do this, we consider the setting of training GFlowNets *offline* and off-policy given a known dataset of final states \mathcal{X} . We sample $x \sim \mathbb{P}_{\mathcal{X}}$, where $\mathbb{P}_{\mathcal{X}}$ is some training distribution over \mathcal{X} . We consider different distributions for $\mathbb{P}_{\mathcal{X}}$ that resemble different practical approaches and techniques that are used for training GFlowNets (see Table 2). This setting controls for the effect of sampling from $P_F(s'|s; \theta)$ in training GFlowNets.

Given a terminal x , we sample a trajectory $\tau = (s_0, \dots, s_f)$ backwards using a uniform P_B^5 . Hence, we term this as *offline* training, since we are avoiding sampling x using $P_F(s'|s; \theta)$. In this way, we are still able to use a standard GFlowNet objective, e.g. SubTB(1), to train $P_F(s'|s; \theta)$ using the backward sampled trajectories. Note that this setup can remove the data non-stationarity that exists during normal training when using on-policy samples from $P(s'|s; \theta)$.

We also wish to assess to what degree deviating from $P_F(s'|s; \theta)$ during training will affect learning $p(x)$. Understanding this may be useful to develop novel GFlowNet algorithms, considering that in practice it seems hard to train models that deviate from on-policy training (Rector-Brooks et al., 2023). To achieve this, we consider a pol-

⁵Investigating the use of different variants/distributions for P_B is another interesting direction that may give insight into the effects of the backward policy on the training dynamics of GFlowNets (see Shen et al., 2023). We leave this for future work.

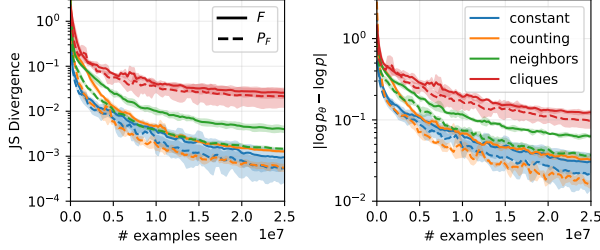


Figure 3. Training a model to distill edge flows and policies on 4 different tasks. It generally seems that (a) doing so recovers the intended distribution fairly well, and (b) modeling P_F appears easier than modeling F , insofar as it recovers $p(x)$ better.

icy interpolation experiment where we sample trajectories from $P_\alpha(s'|s) = (1 - \alpha)P_F(s'|s; \theta) + \alpha P_U(s'|s)$, where $0 \leq \alpha \leq 1$ and $P_U(s'|s)$ denotes a P_F that goes to every terminal state with equal probability, i.e. such that $p(x) \propto 1$. We approximate $P_U(s'|s)$ using a policy pre-trained with a constant reward (thus approximating a uniform $p(x)$).

We then train $P_F(s'|s; \theta)$ *online* instead of *offline*. Note that this is a slightly different setup from what we discussed previously since we re-introduce some of the effects of self-induced training distributions of $P_F(s'|s; \theta)$. We do this because, as we will see, any degree of deviation from $P_F(s'|s; \theta)$ during *offline* training (i.e. sampling $x \sim \mathbb{P}_\mathcal{X}$ and using P_B to construct trajectories) appears to have some negative effect. We observe this even for values of α close to 0. We discuss this in further detail in section 4.4.

This experimental setup helps us investigate the isolated effect of different data distributions $\mathbb{P}_\mathcal{X}$ on training dynamics and generalization by changing the data non-stationarity typically induced by $P(s'|s; \theta)$. To observe the effects on training dynamics, we consider the setting of no test set (the model sees all of \mathcal{X}). In contrast, to observe the effects on generalization, we consider performance on unseen test set examples. This allows us to assess **Hypothesis 1** by observing the effects of various deviations from the normal self-induced training distribution coming from $P_F(s'|s; \theta)$.

4. Experiments

In this section, we report and discuss our observations and findings of the experimental methodology defined in §3. We conduct all experiments reported in this section over 3 random seeds. For training online and offline GFlowNets, we use SubTB(1) and a uniform P_B .

4.1. Distilling Flow Functions

We run the setup explained in §3.1. To evaluate the models, we look at the distributional errors on $p(x; \theta)$. We use a 90%-10% train-test split. We report results in Figure 3 and

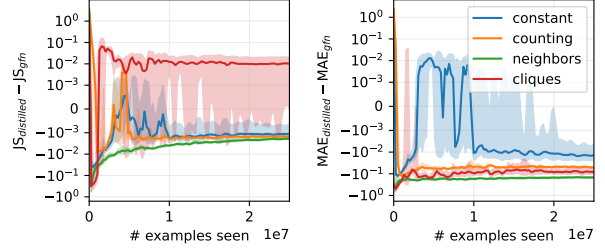


Figure 4. JS-divergence and MAE gaps between SubTB(1) trained GFlowNet model and P_F distilled model. Distilling to P_F generally appears to yield lower distributional error, with the exception of observing JS-divergence on the cliques task.

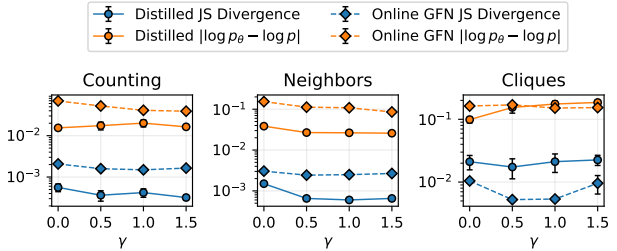


Figure 5. Training models distilled to P_F and GFlowNet models trained online/on-policy for a range of monotonic skew values γ . Transforming the distribution of the reward to contain a larger proportion of high reward values generally does not yield significant influence on performance for approximating $p(x)$.

Figure 4.

First, we can see that learning P_F and learning F yield similar difficulty in the sense that the distributional errors are systematically close across tasks. Second, we see that the model is generalizing, getting sometimes even better scores than a model trained online on the entire states space (i.e. with no test set) as seen in Figure 4. The exception appears to be when evaluating the performance of the cliques task using the JS divergence metric, where the online GFlowNet yields marginally better performance than the distilled models. While expected, this second result is relevant, because it suggests that the difficulty of training a GFlowNet comes from both learning to model the flow functions themselves *and* performing temporal credit assignment.

Observation 4.1. *Flow functions and flow policies are learnable and standard neural networks generalize when predicting them.*

We confirm these observation in sequence and grid environments (see §E.1). We include further results in §D.1 where we assess how well GFlowNets assign probability mass to unvisited states in the graph generation tasks.

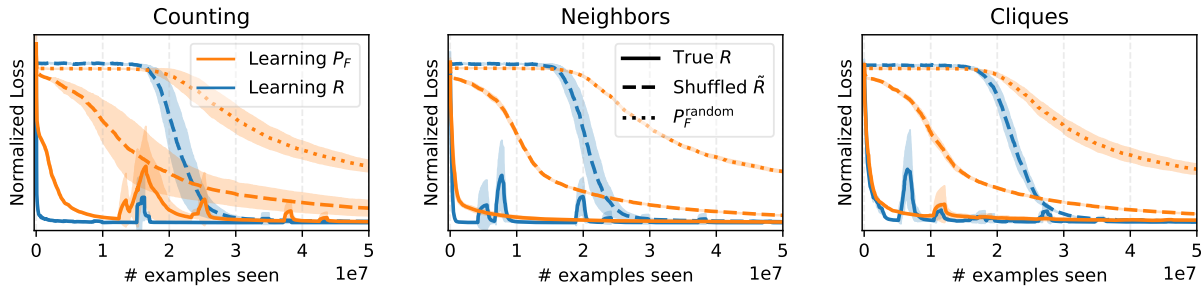


Figure 6. Memorization gap training curves for counting, neighbors, and cliques tasks. Maintaining *flow* structure in the learning problem (learning P_F under shuffled \tilde{R}) induces a smaller *memorization gap* relative to the fully de-structured setting.

4.2. Reward complexity and transformations

Consider a monotonic transform $\mathcal{H}_\gamma : \mathbb{R} \rightarrow \mathbb{R}$ that maps $\log R'(s) = \mathcal{H}_\gamma(\log R(s))$, $\forall s \in \mathcal{S}$ such that $\log R'(s)$ is skewed towards higher reward states as a function of some parameter γ (see §C.3 for further details). We use the setup in §3.1 and also train online GFlowNets in the setting of skewed reward distributions transformed by \mathcal{H}_γ . Results are shown in Figure 5. We observe that as we increase γ (increasing the skewness of the distribution of $\log R$ towards higher reward values), both distilled and online trained models are not significantly affected by the augmented reward distribution.

Observation 4.2. *Monotonic transformations of $R(x)$ do not have detrimental impact on generalization when learning $p(x)$ with GFlowNets.*

This implies that applying minor reward transformations, which is a standard technique in GFlowNet training, is not detrimental to *generalization* about $p(x)$ for a given task (of course, e.g. sparsifying a reward makes exploration harder), supporting **Hypothesis 3**. We repeat this experiment on the sequence environment and find consistent results (see §E.2).

4.3. Memorization Gaps in GFlowNets

We run the setup explained in §3.2 and Table 1; results are shown in Figures 6, with results involving noise corruption⁶ (corrupted constant reward) and online trained GFlowNets included in §D.3. For readers not familiar with the results of Zhang et al. (2021)’s work, a typical observation in the *memorization* setup is for the training loss to initially plateau, until some phase change occurs (one can imagine parameters have self-arranged to create separate linear regions around

⁶This is another setting considered by Zhang et al. (2017; 2021) to achieve de-structuring of the form $s \perp \tilde{R}(s)$.

each input point) and the training loss goes to 0. We observe a similar phenomenon here, regressing to the original R and P_F induce curves with no plateau, while regressing to \tilde{R} and P_F^{random} initially have very flat plateaus until a phase change occurs. This shows a very clear memorization gap, which was expected.

The most interesting result here is where P_F is only partially de-structured, and we regress to the *true* P_F of a shuffled reward \tilde{R} and retain the environment structure information. We observe that while there is no flat plateau, (a) P_F becomes harder to fit and (b) there remains a phase change whereby learning accelerates after some slow period. These results support **Hypothesis 2**; P_F captures structure of both the reward function and the environment, since removing the structure of either induces *memorization gaps*.

Observation 4.3. *The existence of clear memorization gaps, when removing reward structure but maintaining environment structure, suggests that there is informative structure in flow functions and flow policies.*

This finding implies that state flows may play a mechanistic role in *why* GFlowNets generalize to unseen states. In §D.3 we show an extension of these results where we consider rewards corrupted with noise (rather than shuffled). We also show similar results for sequences and grids (see §E.3).

4.4. Generalization in Offline and Off-policy Training of GFlowNets

We run the setup described in §3.3 and Table 2; results on the neighbors task are shown in Figure 7(a) and Figure 7(b). We include full results for all tasks in §D.4. First, we observe that GFlowNets trained in this regime are dependent on environment/task difficulty, the choice of $\mathbb{P}_{\mathcal{X}}$, and on the evaluation metric. For example, the best performing choice

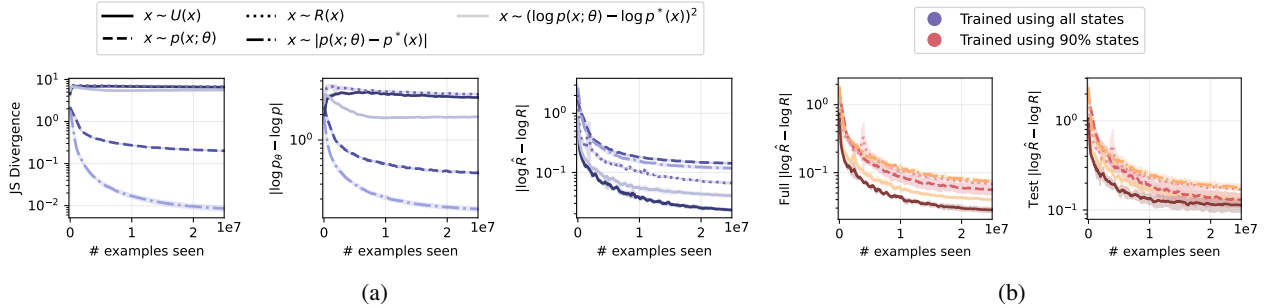


Figure 7. Evaluation curves for offline and off-policy trained GFlowNets on the neighbors task for different choices of $\mathbb{P}_{\mathcal{X}}$. (a) When training using the full dataset (no test set). (b) When training using a subset of the full dataset (90%-10% train-test split). Complete experiments for all graph generation tasks and evaluation metrics are shown in §D.4.

for $\mathbb{P}_{\mathcal{X}}$ on the counting task is typically $x \sim \mathcal{U}$ or $x \sim \log R(x)$, while this is not necessarily the case for neighbors and cliques (see §D.4 Figure 14).

Second, we observe that when training $P_F(s'|s; \theta)$ offline and off-policy in the full data (no test set) regime, convergence rate depends on the choice of $\mathbb{P}_{\mathcal{X}}$ (see Figure 7(a)), sometimes to a catastrophic degree. We see this for our usual distributional metrics for approximating $p(x)$ ⁷. However, when considering the MAE between $\log R(s)$ the approximated $\log \hat{R}(s)$, we do not observe this lack of convergence. We can measure this because GFlowNets learn to implicitly predict the reward: $\log \hat{R}(s) = \log F(s; \theta) + \log P_F(s_f|s; \theta)$. This suggests that although training $P_F(s'|s; \theta)$ offline and off-policy may be tricky, learning $F(s; \theta)$ jointly with $P_F(s'|s; \theta)$ might be beneficial. This is supported by observing a reasonable estimate for $\log \hat{R}(s)$ even when $P_F(s'|s; \theta)$ fails to adequately model $p(x)$ (the model is learning something).

We investigate this finding deeper by considering the off-policy interpolation setup and find that for the more difficult tasks (neighbors and cliques) there exists an apparent trade-off between on-policy and off-policy training when estimating $p(x)$ versus R (see §D.4 Figure 15). In particular, when sampling on-policy (from $P_F(s'|s; \theta)$, $\alpha = 0$), approximating $p(x)$ is reasonable. In contrast, approximating R is best when sampling uniformly off-policy (from $P_{\mathcal{U}}(s'|s)$, $\alpha = 1$) even though error for $p(x)$ is high.

Observation 4.4. *Deviating from the on-policy training distribution induced by $P_F(s'|s; \theta)$ can affect the ability of GFlowNets’ to learn $p(x)$.*

This finding implies that training GFlowNets offline and off-policy may come with challenges depending on the task.

⁷It is possible that the drawbacks of this training regime overwhelm our ability to make meaningful conclusions on the choice of $\mathbb{P}_{\mathcal{X}}$ for offline training on the neighbors and cliques tasks.

However, we observe that the model could be learning some informative structure in $F(s)$ that could help it generalize (seen by reasonable estimates for $\log \hat{R}(s)$). We test this hypothesis in our second offline and off-policy training setup, and we consider performance on an unseen test (see Figure 7(b)). We observe that indeed offline and off-policy trained GFlowNets reasonably approximate R on unseen states even when failing to adequately model $p(x)$.

Observation 4.5. *Learning $F(s)$ is informative to models, who implicitly predict reasonable rewards, even when P_F is unreasonable.*

These results support **Hypothesis 1**; training GFlowNets online and on-policy is ideal, where $P_F(s'|s; \theta)$ converges to sampling trajectories proportional to R . We repeat this experiment (with a left out test set) for the sequence and hypergrid environments. Interestingly, we observe that in these environments $p(x)$ is adequately modelled in the offline and off-policy training regime (see §E.4). This could in-part be due to the reduced complexity of these environments, which we establish by comparing the difficulty of our tasks to the difficulty of fitting the constant reward (see §E.1).

5. Conclusion

In this work, we conducted an empirical investigation into the generalization behaviours of GFlowNets. We introduced a set of graph generation tasks of varying difficulty to benchmark and measure GFlowNet generalization performance. Our findings support existing hypothesized *mechanisms* of generalization of GFlowNets as well as add to our understanding of *why* GFlowNets generalize. We found that GFlowNets inherently learn to approximate functions which contain structure favourable for generalization. In addition, we found that the reward implicitly learned by GFlowNets is robust to changes in the training distribution, but that GFlowNets are sensitive to being trained off-policy. We discuss limitations and future directions of this work in §B.

Impact Statement

The outcomes of the research conducted in this work have practical implications for generative modelling in applications that include drug discovery, material design, and general combinatorial optimization in commercial settings. Because of this, we recognize the importance of considering safety and alignment in these closely related domains. We believe that advancements in GFlowNet research could result in models with improved generalization, in turn leading to models that are easier to align. Another important and useful application of GFlowNets is in the causal and reasoning domains. We believe that advancements in these areas may lead to more interpretable, easier to understand, and safer models. Lastly, we highlight that the applications of our findings for the advancements of GFlowNets may rely on building upon the hypotheses put forward in this work.

Acknowledgments

The bulk of this research was done at Valence Labs as part of an internship, using computational resources there. The authors are grateful to Yoshua Bengio, Berton Earnshaw, Dinghui Zhang, Johnny Xi, Jason Hartford, Philip Fradkin, Cristian Gabellini, Julien Roy, and the Valence Labs team for fruitful discussions and feedback. In addition, we acknowledge funding from the Natural Sciences and Engineering Research Council of Canada and the Vector Institute.

References

- Arpit, D., Jastrzebski, S., Ballas, N., Krueger, D., Bengio, E., Kanwal, M. S., Maharaj, T., Fischer, A., Courville, A., Bengio, Y., et al. A closer look at memorization in deep networks. In *International Conference on Machine Learning*. PMLR, 2017.
- Atanackovic, L., Tong, A., Wang, B., Lee, L. J., Bengio, Y., and Hartford, J. DynGFN: Towards bayesian inference of gene regulatory networks with gflownets. In *Thirty-seventh Conference on Neural Information Processing Systems*, 2023.
- Bengio, E., Pineau, J., and Precup, D. Interference and generalization in temporal difference learning. In *International Conference on Machine Learning*. PMLR, 2020.
- Bengio, E., Jain, M., Korablyov, M., Precup, D., and Bengio, Y. Flow network based generative models for non-iterative diverse candidate generation. *Advances in Neural Information Processing Systems*, 34:27381–27394, 2021.
- Bengio, Y., Lahlou, S., Deleu, T., Hu, E. J., Tiwari, M., and Bengio, E. Gflownet foundations. *Journal of Machine Learning Research*, 24(210):1–55, 2023.
- Cobbe, K., Klimov, O., Hesse, C., Kim, T., and Schulman, J. Quantifying generalization in reinforcement learning. In *International Conference on Machine Learning*, pp. 1282–1289. PMLR, 2019.
- Deleu, T., Góis, A., Emezue, C., Rankawat, M., Lacoste-Julien, S., Bauer, S., and Bengio, Y. Bayesian structure learning with generative flow networks. In *Uncertainty in Artificial Intelligence*, pp. 518–528. PMLR, 2022.
- Deleu, T., Nishikawa-Toomey, M., Subramanian, J., Malkin, N., Charlin, L., and Bengio, Y. Joint bayesian inference of graphical structure and parameters with a single generative flow network. *arXiv preprint arXiv:2305.19366*, 2023.
- Jain, M., Bengio, E., Hernandez-Garcia, A., Rector-Brooks, J., Dossou, B. F., Ekbote, C. A., Fu, J., Zhang, T., Kilgour, M., Zhang, D., et al. Biological sequence design with gflownets. In *International Conference on Machine Learning*, pp. 9786–9801. PMLR, 2022.
- Jain, M., Raparthy, S. C., Hernández-García, A., Rector-Brooks, J., Bengio, Y., Miret, S., and Bengio, E. Multi-objective gflownets. In *International Conference on Machine Learning*, pp. 14631–14653. PMLR, 2023.
- Kawaguchi, K., Kaelbling, L. P., and Bengio, Y. Generalization in deep learning. *arXiv preprint arXiv:1710.05468*, 1(8), 2017.
- Lahlou, S., Deleu, T., Lemos, P., Zhang, D., Volokhova, A., Hernández-García, A., Ezzine, L. N., Bengio, Y., and Malkin, N. A theory of continuous generative flow networks. In *International Conference on Machine Learning*, pp. 18269–18300. PMLR, 2023.
- Leshno, M., Lin, V. Y., Pinkus, A., and Schocken, S. Multilayer feedforward networks with a nonpolynomial activation function can approximate any function. *Neural networks*, 6(6):861–867, 1993.
- Li, G., Xiong, C., Thabet, A., and Ghanem, B. Deepergcn: All you need to train deeper gcns. *arXiv preprint arXiv:2006.07739*, 2020.
- Ma, G., Bengio, E., Bengio, Y., and Zhang, D. Baking symmetry into gflownets. In *NeurIPS 2023 AI for Science Workshop*, 2023.
- Madan, K., Rector-Brooks, J., Korablyov, M., Bengio, E., Jain, M., Nica, A., Bosc, T., Bengio, Y., and Malkin, N. Learning gflownets from partial episodes for improved convergence and stability. *arXiv e-prints*, page. *arXiv preprint arXiv:2209.12782*, 2022.

- Malkin, N., Jain, M., Bengio, E., Sun, C., and Bengio, Y. Trajectory balance: Improved credit assignment in gflownets. *Advances in Neural Information Processing Systems*, 35:5955–5967, 2022.
- Nica, A. C., Jain, M., Bengio, E., Liu, C.-H., Korablyov, M., Bronstein, M. M., and Bengio, Y. Evaluating generalization in gflownets for molecule design. In *ICLR2022 Machine Learning for Drug Discovery*, 2022.
- Packer, C., Gao, K., Kos, J., Krähenbühl, P., Koltun, V., and Song, D. Assessing generalization in deep reinforcement learning. *arXiv preprint arXiv:1810.12282*, 2018.
- Pan, L., Malkin, N., Zhang, D., and Bengio, Y. Better training of gflownets with local credit and incomplete trajectories. In *International Conference on Machine Learning*, 2023.
- Pascanu, R., Montufar, G., and Bengio, Y. On the number of response regions of deep feed forward networks with piece-wise linear activations. *arXiv preprint arXiv:1312.6098*, 2013.
- Rector-Brooks, J., Madan, K., Jain, M., Korablyov, M., Liu, C.-H., Chandar, S., Malkin, N., and Bengio, Y. Thompson sampling for improved exploration in gflownets. *arXiv preprint arXiv:2306.17693*, 2023.
- Shen, M. W., Bengio, E., Hajiramezanali, E., Loukas, A., Cho, K., and Biancalani, T. Towards understanding and improving gflownet training. *arXiv preprint arXiv:2305.07170*, 2023.
- Shi, Y., Huang, Z., Feng, S., Zhong, H., Wang, W., and Sun, Y. Masked label prediction: Unified message passing model for semi-supervised classification. *arXiv preprint arXiv:2009.03509*, 2020.
- Tossou, P., Wognum, C., Craig, M., Mary, H., and Noutahi, E. Real-world molecular out-of-distribution: Specification and investigation. 2023.
- Vaswani, A., Shazeer, N., Parmar, N., Uszkoreit, J., Jones, L., Gomez, A. N., Kaiser, Ł., and Polosukhin, I. Attention is all you need. *Advances in neural information processing systems*, 30, 2017.
- Veličković, P., Cucurull, G., Casanova, A., Romero, A., Lio, P., and Bengio, Y. Graph attention networks. *arXiv preprint arXiv:1710.10903*, 2017.
- Zhang, A., Ballas, N., and Pineau, J. A dissection of overfitting and generalization in continuous reinforcement learning. *arXiv preprint arXiv:1806.07937*, 2018.
- Zhang, C., Bengio, S., Hardt, M., Recht, B., and Vinyals, O. Understanding deep learning requires rethinking generalization. In *International Conference on Learning Representations*, 2017.
- Zhang, C., Bengio, S., Hardt, M., Recht, B., and Vinyals, O. Understanding deep learning (still) requires rethinking generalization. *Communications of the ACM*, 64(3):107–115, 2021.
- Zhang, D., Malkin, N., Liu, Z., Volokhova, A., Courville, A., and Bengio, Y. Generative flow networks for discrete probabilistic modeling. In *International Conference on Machine Learning*, pp. 26412–26428. PMLR, 2022.

A. Vocabulary

- **The $p(x; \theta)$ distribution**, when using GFNs we never explicitly model $p(x; \theta)$; instead this measure is induced by the parameterization ($F(s \rightarrow s'; \theta)$ or $P_F(s'|s; \theta)$) of a sequential constructive policy. We use $p(x; \theta)$ as the shorthand for *the distribution over X induced by the chosen parameterization with parameters θ* . See also §C.1.2.
- **Online vs offline**, a model is trained online when it is trained from data generated during the training process – typically according to its own parameters, i.e. for some model $p(x; \theta)$, we may use $X \sim p(x; \theta)$ to train $p(x; \theta)$. Conversely a model trained offline is trained from a (usually fixed) data set, $X \sim \mathcal{D}$. It is possible to form a mixture of online and offline data. GFNs are compatible with this paradigm (unlike RL methods such as policy gradient methods).
- **On-policy vs off-policy**, a model is trained on-policy if it is trained from data generated according to the unperturbed distribution $p(x; \theta)$, whereas it is trained off-policy if it comes from any other distribution. For example, taking some actions at random would be considered off-policy (although a mild version), but so would taking samples from an entirely different distribution $p(x; \theta')$ or from a dataset.
- **Self-induced distribution**, when training a model we refer to the distribution $p(x; \theta)$ as “self-induced”. This is mainly to emphasize that this distribution changes as θ changes, which in online on-policy contexts is due to the model generating its *own* training samples (thus the “self”-induced).

B. Limitations and Future Work

Limitations: We have shown that GFlowNets tend to generalize when learning unnormalized probability mass functions for approximating $p(x)$ over discrete spaces. In particular, we have investigate the generalization behaviours of GFlowNets in the context of distributional errors for $p(x)$. Because of the combinatorial nature of computing $p(x)$ exactly, and likewise computing $p(x; \theta)$ from $P(s'|s; \theta)$, we are limited in the fact that we need to work within reasonably sized discrete spaces (as those we have proposed) to study GFlowNet generalization for approximating $p(x)$. Secondly, we don’t explicitly test generalization in online and on-policy trained GFlowNets. This in part a consequence of requiring an environment and state space large enough such that a sufficient quantity of unseen states can be produced, while also being able to purposely hide the visited states from parameters updates of the GFlowNet. Lastly, although our proposed problems and environments have structure that induces difficult and interesting generalization tasks, they still may remain far from the structure of the real world.

Future Directions: We hope to have formed a sound set of findings and observations that may lead to future research in understanding and formalizing generalization in GFlowNets. For instance, our set of findings could be used as starting points for formalizing some of our notions and intuitions for GFlowNet generalization (and the corresponding mechanisms) into mathematical theory. Another direction that can stem from our work is to further empirically investigate GFlowNet generalization in the online and on-policy setting. Since we don’t explicitly look at GFlowNet generalization in the online and on-policy training regime (i.e. since we don’t hide any states from online trained GFlowNets); it would be interesting in future work to explicitly investigate this. However, it is important to note that this is not necessarily a trivial task (as described in limitations).

C. Experimental Details

C.1. Details for constructing graph benchmark task

C.1.1. REWARD FUNCTIONS

Here are the exact log-reward functions we use, as implemented in Python using the `networkx` (nx) and `numpy` (np) libraries.

cliques counts the number of 4-cliques in a graph such that at least 3 of the 4 nodes of the cliques share the same color. We then subtract to that number the total number of cliques in the graph, but add the number of nodes. This is so that the maximal log-reward is 0. We clip log-rewards below -10.

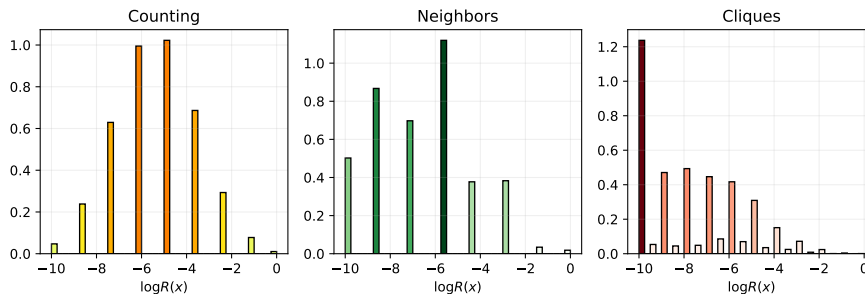


Figure 8. Distribution of log rewards for the given tasks: (left) **counting**, (middle) **neighbors**, and (right) **cliques**.

```
def cliques(g, n=4):
    cliques = list(nx.algorithms.clique.find_cliques(g))
    # The number of cliques each node belongs to
    num_cliques = np.bincount(sum(cliques, []))
    colors = {i: g.nodes[i]["v"] for i in g.nodes}

    def color_match(c):
        return np.bincount([colors[i] for i in c]).max() >= n - 1

    cliques_match = [float(len(i) == n) * (1 if color_match(i) else 0.5) for i in cliques]
    return np.maximum(np.sum(cliques_match) - np.sum(num_cliques) + len(g) - 1, -10)
```

neighbors looks at all the neighbors of every node, counting the number of nodes with an even number of neighbors of the opposite color. This total is modified as a function of the number of nodes in order to produce a nice log-reward distribution between 0 and -10.

```
def neighbors(g):
    total_correct = 0
    for n in g:
        num_diff_colr = 0
        c = g.nodes[n]["v"]
        for i in g.neighbors(n):
            num_diff_colr += int(g.nodes[i]["v"] != c)
        total_correct += int(num_diff_colr % 2 == 0) - (1 if num_diff_colr == 0 else 0)
    return np.float32((total_correct - len(g.nodes) if len(g.nodes) > 3 else -5) * 10 / 7)
```

counting simply counts the number of red and green nodes, red nodes being "worth" more, and again modifies this count in order to produce a nice 0 to -10 log-reward distribution.

```
def counting(g):
    ncols = np.bincount([g.nodes[i]["v"] for i in g], minlength=2)
    return np.float32(-abs(ncols[0] + ncols[1] / 2 - 3) / 4 * 10)
```

C.1.2. COMPUTING $p(x; \theta)$, $F(s)$, $F(s \rightarrow s')$, AND P_F

We compute the probability of a model with parameters θ sampling x , $p(x; \theta)$ via what is essentially Dynamic Programming. We visit states s in **topological order** starting from s_0 . For every child of s , s' , (valid transition $s \rightarrow s'$) we add $p_v(s)P_F(s'|s; \theta)$ to the probability of visiting $p_v(s')$, eventually accumulating visitation probability from all the parents of s' . This is possible because we are visiting states in topological order. Note that we start with $p_v(s_0) = 1$ and p_v set to 0 for every other state. $p(s; \theta)$ is computed as $p_v(s)P_F(\text{stop}|s)$.

The above is fairly easy to batch, requires one forward pass per state. Computing P_F is the most expensive operation and can be batched, as long as values are accumulated by respecting a topological order afterwards. We also actually store values on a log scale, using logaddexp operations for numerical stability.

To compute *true* flow functions, we do the reverse, visiting the DAG in reverse topological order. For every state s , we add $F(s)P_B(s'|s)$ units of flow to every parent s' of s , starting at leaves (due to the reverse topological order) where $F(s) = R(s)$. We similarly set the value of the edge flow $F(s \rightarrow s') = F(s)P_B(s'|s)$. P_F is simply the softmax of edge flows. Note that we use a uniform P_B , as explained in the main text.

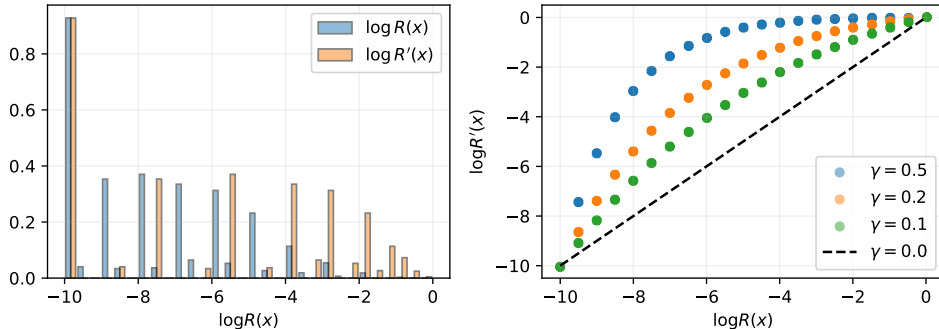


Figure 9. Example of monotonic transform \mathcal{H}_γ . (left) distributions of $\log R(x)$ and $\log R'(x)$ for true log-rewards and skewed log-rewards (using $\gamma = 0.2$). (right) plot of $\log R(x)$ versus $\log R'(x)$ for various values of γ . Points above the $\gamma = 0$ line yield skew towards higher log-reward values.

C.1.3. CONSTRUCTING TEST SET

Why 6 nodes? Considering the maximal number of nodes is 7, 6 may seem “too close”. On the other hand, picking a graph and excluding its subtree means that this subgraph will *never* appear in the training set. This is quite aggressive, for example creating a test set of 10% of the data only requires 35 such graphs whose subtrees are excluded. These graphs have an average of 272 ± 205 descendants. Choosing graphs of 5 nodes would exclude an average of ~ 4700 graphs per pick, meaning that a test set of 10% of the data would only stem from the exclusion of 2 or 3 graphs. This may not have the diversity we desire, thus our choice of 6 nodes.

Finally, we believe this is an interesting choice that relates to real-world applications of GFlowNets. In drug-discovery of small molecules, given the enormous size of the state space, it is likely for most subgraphs of a sufficient size to never appear in the training set (because a model can only train for so many iterations in practice). In a graph generation context we are thus interested in how a model generalizes to subgraphs it’s never seen. In this proposed benchmark, 67994 of the 72296 states are graphs of 7 nodes; only excluding graphs of 6 or 7 nodes thus covers most of state space.

C.2. Details for hypergrid and sequence environments and tasks

C.2.1. $(M \times M)$ HYPERGRID:

Grid environments have been used in GFlowNet papers since their inception (Bengio et al., 2021) as a sanity check environment, presumably inheriting this custom from Reinforcement Learning. We continue the tradition and report results on a 2D grid environment. In it, the agent has 3 actions, move in the $x+$ direction, move in the $y+$ direction, or stop. The agent navigates on a grid of size M (64 in our experiments), and is forced to stop if any of the coordinates reaches $M - 1$.

As a reward signal we use functions used in past work (Bengio et al., 2021; Jain et al., 2023).

C.2.2. BIT SEQUENCES:

Auto-regressive sequence environments have been used in a variety of past GFlowNet work (Malkin et al., 2022; Madan et al., 2022; Pan et al., 2023). In this work, we consider a bit sequence environment akin to that originally introduced by Malkin et al. (2022). We consider a reward of the form $R(x) = \exp\left(-\frac{\min_{m \in \mathcal{M}} d(x, m)}{l}\right) \times 10$, where d is the Levenshtein edit distance between an input sequence x and the closest “mode” sequence m , $\mathcal{M} \subset \mathcal{X}$ is the set of mode-sequences, and l is the max sequence length. We select $|\mathcal{M}| = 60$ sequences from \mathcal{M} uniformly at random given the set \mathcal{X} of all possible bit sequences up to length $l = 15$ to be the “mode” sequences (we do this once at the start of each run). This yields a discrete state space of 65,535 states, comparable in size to our graph generation environment.

C.3. Monotonic reward transformation

We consider a monotonic transform of the form $\mathcal{H}_\gamma(\log R(x)) = \log R(x)e^{(-\gamma \log R(x))}$. As described earlier, the transform \mathcal{H}_γ maps $\log R'(s) = \mathcal{H}_\gamma(\log R(s))$, $\forall s \in \mathcal{S}$ such that $\log R'(s)$ is skewed towards higher reward states as a function of

some parameter γ (see §C.3 for further details. Note, \mathcal{H}_γ is monotonic for values of $\log R(x) \leq 0$ and $\gamma \geq 0$. In our graph and sequence generations tasks, $\log R(x) \leq 0, \forall x \in \mathcal{X}$, hence we are able to use \mathcal{H}_γ as a monotonic transform for $\log R(x)$. We show an example of \mathcal{H}_γ applied to the cliques task in Figure 9 for various value sof γ .

C.4. Evaluation metrics

To measure the generative modelling performance of GFlowNets we consider the Jensen-Shannon (JS) divergence and the MAE between the learned $\log p(x; \theta)$ and the true $\log p(x)$. For JS divergence, we compute:

$$\text{JS}(p(x), p(x; \theta)) = \frac{1}{2} \text{KL}(p(x) \| Q) + \frac{1}{2} \text{KL}(p(x; \theta) \| Q), \quad (3)$$

where $Q = \frac{1}{2}(p(x) + p(x; \theta))$. This reduces to

$$\text{JS}(p(x), p(x; \theta)) = \frac{1}{2} \sum_{x \in \mathcal{X}} (p(x; \theta)(\log p(x; \theta) - \log p(x)) + p(x)(\log p(x) - \log p(x; \theta))). \quad (4)$$

For the MAE, we simply take the absolute error $|\log p(x; \theta) - \log p(x)|$ and average over the cardinality of the state space.

C.5. Model architectures

For all graph experiments we use a modified graph transformer (Veličković et al., 2017; Shi et al., 2020). On top of the normal attention mechanism, we augment the input of each layer with the output of one round of message passing (using layers from the work of Li et al., 2020) with a `sum` aggregation—we found that this was useful in tasks where counting was required. We use 8 layers with 128-dimensional embeddings and 4 attention heads; we use this architecture after having tried different numbers of layers and embeddings in order to validate our task; this is coincidentally represented in Fig. 1.

For sequence tasks, we use a vanilla transformer (Vaswani et al., 2017) with 4 layers of 64 embeddings and 2 attention heads. We did not search for hyperparameters, since this setup has been used in prior work (Malkin et al., 2022).

For grid tasks we use a LeakyReLU MLP with 3 layers of 128 units. The input is a one hot representation of each coordinate.

C.6. Implementation details

Our experiments are implemented in Pytorch and Pytorch Geometric. Our code is available at <https://github.com/lazaratan/gflownet-generalization>.

D. Additional Graph Task Experiments

D.1. GFlowNets learn rank preservation of unseen states

Task	Supervised	Distilled F	Distilled P_F	offline TB	offline subTB	offline FM
	Test set Spearman correlation					
cliques	0.92 ± 0.02	0.92 ± 0.01	0.93 ± 0.00	0.88 ± 0.01	0.90 ± 0.01	0.86 ± 0.03
neighbors	0.98 ± 0.00	0.98 ± 0.00	0.98 ± 0.00	0.96 ± 0.00	0.96 ± 0.00	0.96 ± 0.00
count	0.98 ± 0.00	0.98 ± 0.00	0.98 ± 0.00	0.95 ± 0.01	0.95 ± 0.00	0.96 ± 0.00
	Test set top-100 Spearman correlation					
cliques	0.66 ± 0.02	0.74 ± 0.10	0.83 ± 0.04	0.67 ± 0.10	0.69 ± 0.11	0.53 ± 0.13
neighbors	0.87 ± 0.00	0.87 ± 0.00	0.87 ± 0.00	0.86 ± 0.01	0.86 ± 0.00	0.86 ± 0.01
count	0.44 ± 0.00	0.44 ± 0.00	0.44 ± 0.00	0.24 ± 0.06	0.24 ± 0.06	0.37 ± 0.02
	Avg Rank of optimal objects					
cliques (15)	21.5 ± 14.5	39.3 ± 30.2	13.3 ± 5.3	18.1 ± 4.9	12.1 ± 2.0	17.7 ± 5.2
neighbors (48)	23.5 ± 0.0	23.5 ± 0.0	23.5 ± 0.0	43.4 ± 5.5	43.6 ± 9.4	40.7 ± 2.2
count (7)	3.0 ± 0.0	3.0 ± 0.0	3.0 ± 0.0	62.7 ± 12.3	61.1 ± 15.1	25.6 ± 4.2

Table 3. Comparing the rankings given by different ways of training a model on a dataset. Standard deviations are over 4 runs. In the last three rows the number in brackets is the number of optimal objects in the test set.

We want to assess more precisely where GFNs put probability mass, in particular in states they’ve never visited. More specifically though, GFNs are often used to find *likely* hypotheses, i.e. generate objects “close enough” to the argmax(es).

Consider the following scenario, which is a common way to use GFNs. Some dataset of objects and scores $\mathcal{D} = \{(x_i, y_i)\}$ is given to us. We train a reward proxy to regress to $R(x_i; \theta) = y_i$, and then train a GFN on $R(x; \theta)$ in order to generate x s (and commonly, find the most “interesting” x). If we assume that supervised learning is “as good as it gets” to approximate R , then the task of finding $\arg \max_x R(x)$ by finding $\arg \max_x R(x; \theta)$ should also be as good as it gets. This prompts us to ask, how close are GFNs to this ideal?

In the following experiment, we look at three measures. First, the Spearman rank correlation on the probabilities $p(x; \theta)$ (or $R(x; \theta)$ for the supervised model) of the test set, second we do the same for the top-100 graphs in the test set, and finally we look at the mean rank of the set of optimal x s in the test set (e.g. if there are 7 optimal graphs in the test set and the model perfectly predicts their rank to be $[0, 1, 2, 3, 4, 5, 6]$ then the mean rank is $(0 + 1 + 2 + \dots + 6)/7 = 3.0$).

These measures are intended to be proxies for how likely it is that a model trained on some dataset would be able to generate objects close enough to the optimal objects.

This third measure is also inspired by the following fact: it has been observed in a few setups that even though trajectory balance objectives appeared to fit the distribution much better than flow matching, flow matching can be more efficient at producing high-reward samples (which seems counter-intuitive).

We thus compare distilling edge flows to policies, as well as TB objectives to the FM objective. Specifically for GFN objectives (TB, subTB, FM), we use an offline paradigm where we sample trajectories by sampling an x uniformly at random from \mathcal{D} and going backwards with P_B uniformly at random (this is presumably a somewhat ideal training condition).

We report the results in Table 3. The results are quite dense, so let us make a few observations:

- When considering the entire test set, the supervised model is indeed the gold standard. Offline GFN models are slightly worse. This isn’t too surprising, and is in fact reminiscent of results related to the difficulty of training value functions via TD in RL (Bengio et al., 2020).
- When considering either the top-100 or the optimal objects, we see surprising results for the cliques task (the hardest task)
 - for the top-100 objects, the distilled models do better, and the offline TB models are on-par with (and occasionally better than) the supervised model
 - for the rank of optimal objects, not only does distilled P_F do better, the offline GFN methods do better as well.
 Recall that some test set information is leaking into training; it may explain the advantage of distilled models, but not the advantage of offline GFN models.
- TB and subTB are generally better at fitting *ranking* than FM, *except* when it comes to optimal objects. This reproduces past observations, suggesting flow matching over-weights high-reward states, even outside of its training data; we unfortunately do not have a coherent explanation:
 - $F(s, s')$ distillation being worse than P_F distillation means modeling F is probably not the advantage;
 - This phenomenon is consistent across training, although not on every task.
 - This phenomenon is amplified when *not* correcting for idempotent actions. This is expected (Ma et al., 2023), but useful to measure.

We repeat these three measures with different train-test ratios, shown in Figure 19, where we see that the results are as expected, and consistent with Table 3. To summarize: *GFlowNets implicitly learn to put more mass on high-reward objects than low-reward objects outside their training set.*

The above is interesting, but is still just a statement about *ranking* between unseen states. Obviously this says nothing about the total probability mass given to unseen states.

D.2. Distilled flow experiments over only unseen states

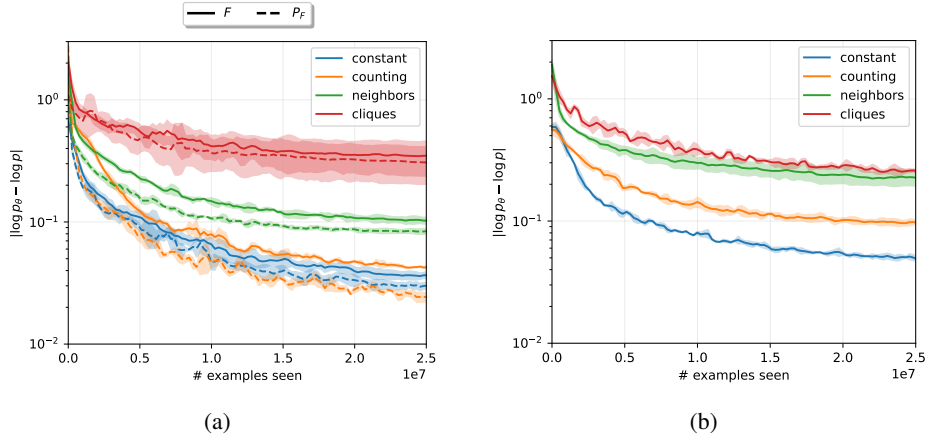


Figure 10. MAE error for only unseen states on constant, counting, neighbors, and clique graph generations tasks. (a) evaluation for model trained to distill edge flows and policies. (b) evaluation an online trained GFlowNet via SubTB(1). We see that considering only the unseen states for MAE metric leads to comparable observation to the case of evaluating MAE over all states. This is expected since error on the unseen states should be driving the model’s overall evaluation performance when evaluating on the entire state space. Note, for the online GFlowNet, there is no guarantee that the model has not “seen” the left out unseen states in this evaluation.

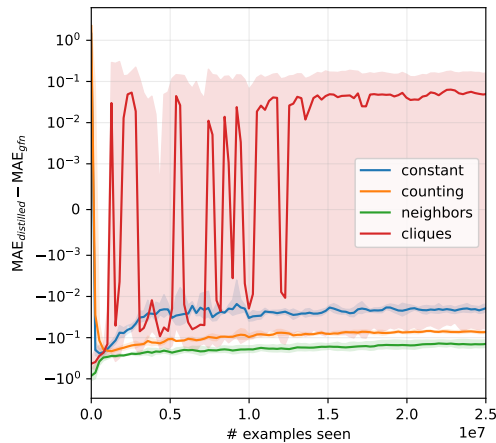


Figure 11. MAE gap between online trained GFlowNet via SubTB(1) and distillation trained model regressing to P_F on only unseen states. We observe that when considering only unseen states, results are consistent with evaluation over the entire state space. This is also expected since error on the unseen states should be driving the model’s overall evaluation performance when evaluating on the entire state space.

D.3. Additional memorization experiments

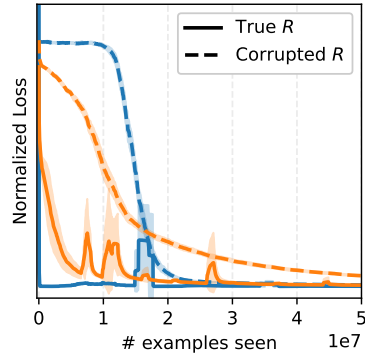


Figure 12. Memorization gap training curves for the constant reward on the graph generation task. In this experiment, we consider the case where Gaussian noise corrupts the constant reward signal of the form $\tilde{R}(x) = R(x) + \epsilon, \epsilon \sim \mathcal{N}(0, \sigma)$, thus inducing de-structuring. Here we consider $\sigma = 2$. We observe behaviour consistent with that found in §4.3.

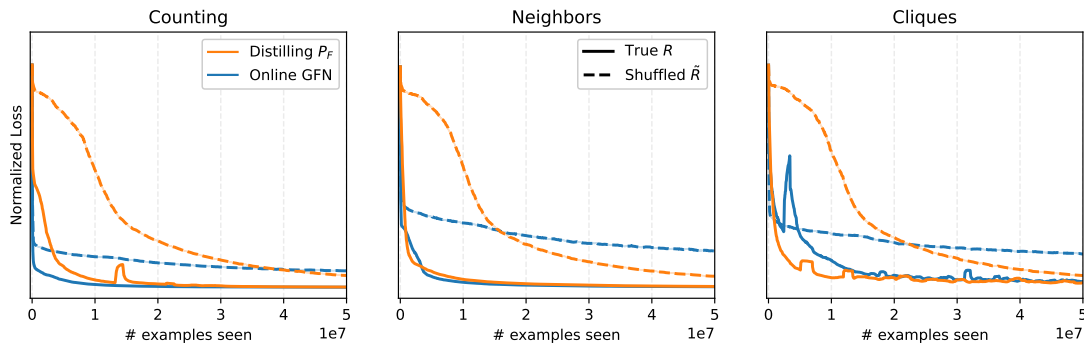


Figure 13. Memorization gap training curves for counting, neighbors, and cliques tasks for distilled (regressing to P_F) and online trained GFlowNet. We observe results are consistent with findings in §4.3 for the online trained GFlowNet.

D.4. Full Experimental results for offline and off-policy training of GFlowNets

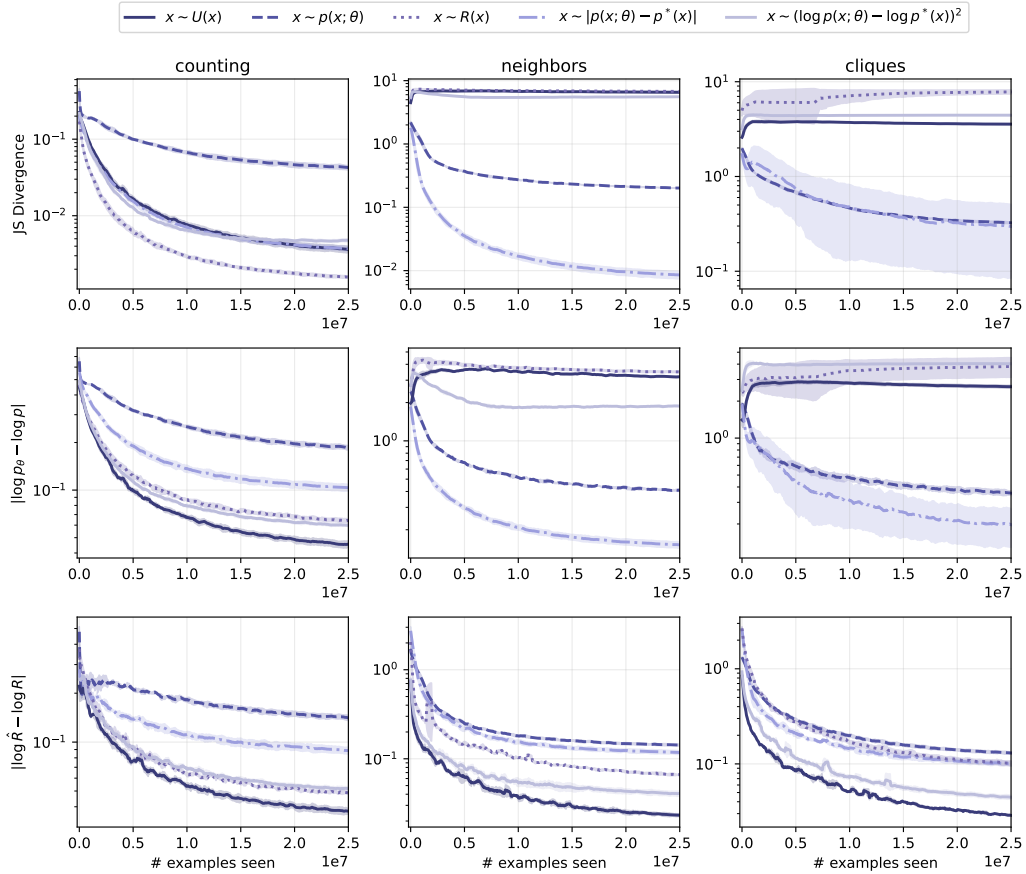


Figure 14. Evaluation curves for offline and off-policy trained GFlowNets on counting, neighbors, and cliques graph generations tasks for different choices of $\mathbb{P}_{\mathcal{X}}$ when training using the full dataset (no test set). Model performance is dependent on the choice of $\mathbb{P}_{\mathcal{X}}$. When considering evaluation on the JS divergence and MAE metrics, depending on task and some choices of $\mathbb{P}_{\mathcal{X}}$, $p(x)$ is not adequately approximated. However, regardless of task, offline and off-policy trained GFlowNets appear to robustly learn R .

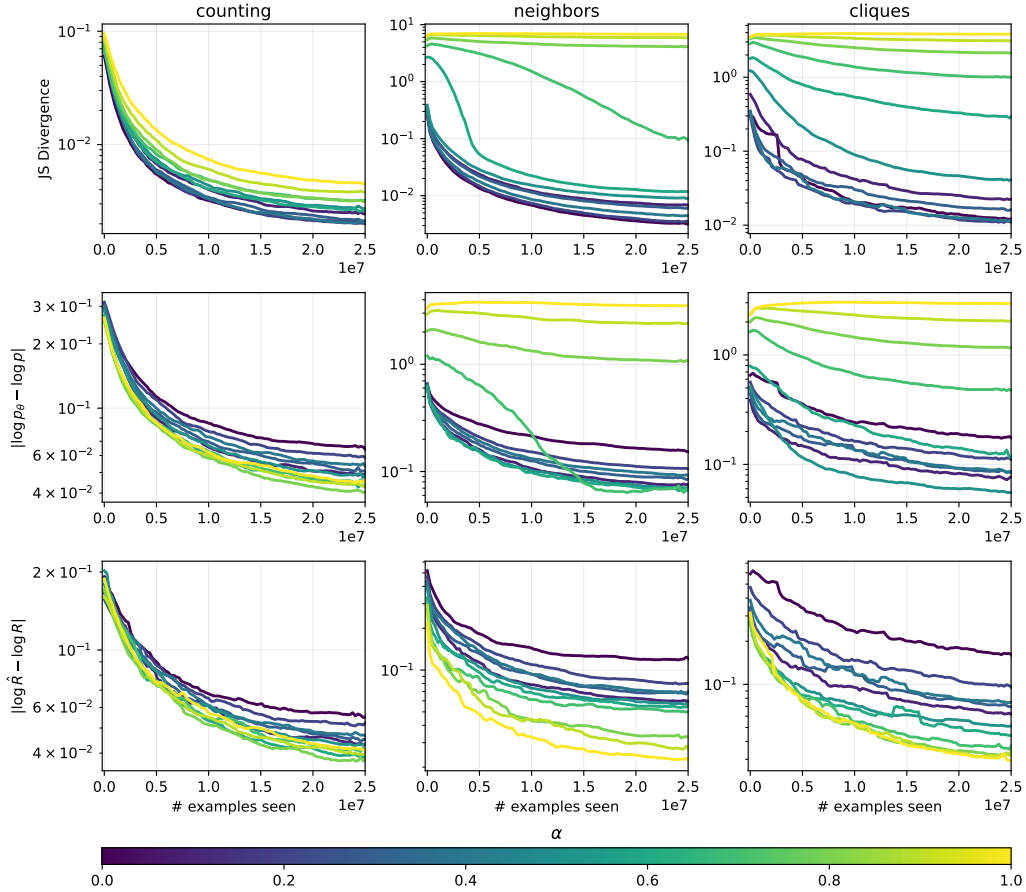


Figure 15. Results for policy mixing interpolation experiments. Here, we mix $P_\alpha(s'|s) = (1 - \alpha)P_F(s'|s; \theta) + \alpha P_U(s'|s)$, where $0 \leq \alpha \leq 1$. For $\alpha = 0$, the model is fully on-policy, sampling trajectories from $P_F(s'|s; \theta)$. For $\alpha = 1$, the model is sampling fully off-policy using $P_U(s'|s)$. This approximates the behaviour of training offline and off-policy when using $x \sim \mathcal{U}(x)$ (i.e. uniform sampling of x). Here we can observe the effects of deviating from on-policy samples during training. We see that at times, specifically for the more difficult tasks (neighbors and cliques), even small degrees of deviation from $P_F(s'|s; \theta)$ can lead to worsened performance when approximating $p(x)$ (seen by sensitivity in distributional JS divergence and MAE metrics). In contrast, approximating R appears to improve as the model samples more uniformly over \mathcal{X} (if not entirely uniform, i.e. when $\alpha = 1$). Interestingly, the counting task appears generally invariant to minor changes in α .

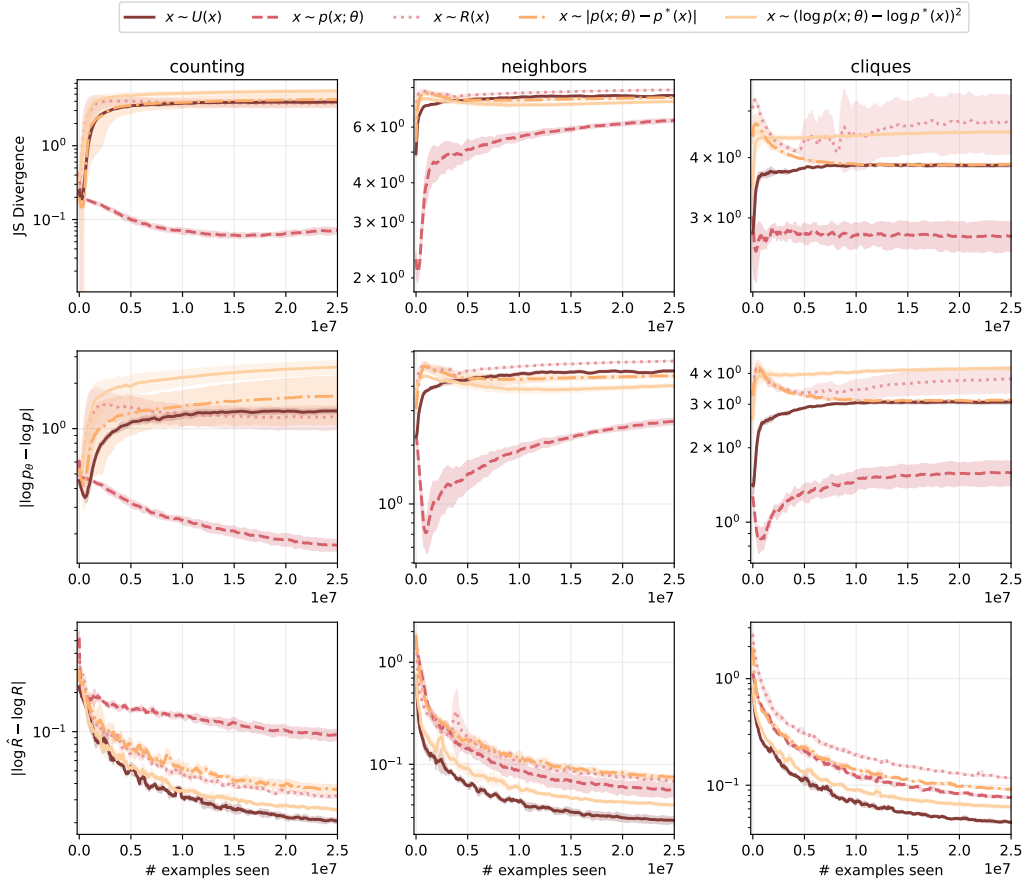


Figure 16. Evaluation curves for offline and off-policy trained GFlowNets on counting, neighbors, and cliques graph generations tasks for different choices of $\mathbb{P}_{\mathcal{X}}$ when training using a subset of the full dataset (90%-10% train-test split). In this setting, agnostic to the choice of $\mathbb{P}_{\mathcal{X}}$ and graph generation task, we observe the GFlowNet models struggles to converge when considering JS divergence and MAE distributional metrics for approximating $p(x)$. However, we observe the GFlowNet models remains robust when learning R .

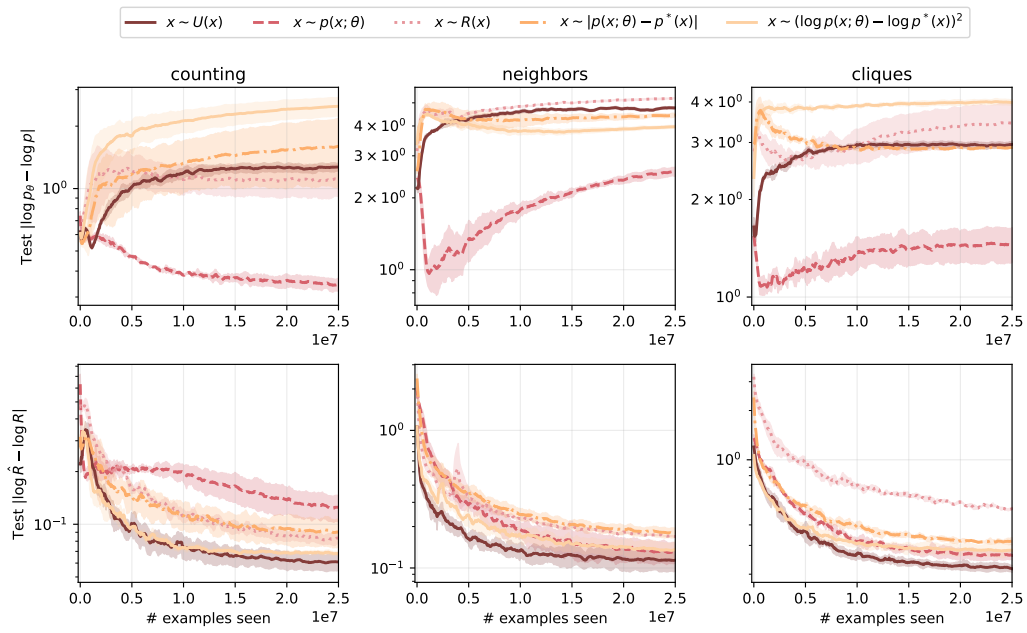


Figure 17. Continuation of Figure 16, but evaluated over only the unseen states (test states). We observe performance is consistent with the evaluations over the entire state space (Figure 16).

D.5. Offline GFlowNets inadequately assign probability mass

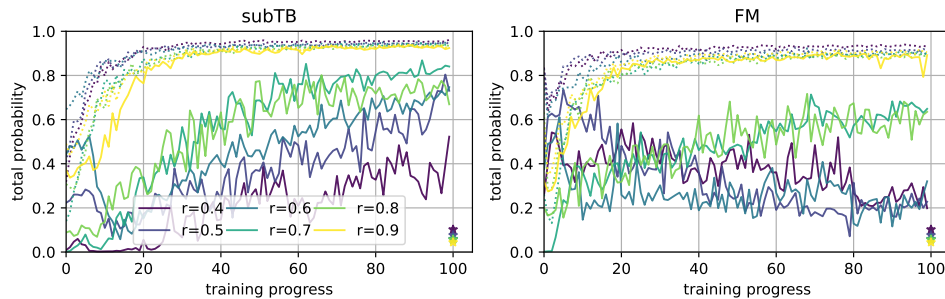


Figure 18. The total probability of the test set (dotted) and of the top-100 objects within the test set (full lines); means of 4 seeds. Each color is a different training/test split ratio. As the model has access to more data, it seems to overfit *more*; it gives more total probability to very few states, but particularly, to high reward states. We also plot in the bottom right (stars) what the “true” total probability of the top-100 objects should be (it varies because of the random seeds and test set size, we show the seed average).

Let’s dig into the experiment of §D.1. We’ve established that offline GFNs manage to rank unseen states fairly well, but this says nothing about how much probability it gives those states, only that the relative probabilities are well behaved.

In Figure 18 we show how much *total probability* (i.e. $\sum_{i \in \text{test}} p(x_i; \theta)$) is allocated to the test set. In particular, we show the total probability of the whole test set, as well as of the top-100 objects within the test set.

We believe the following result is unexpected: **as the training set grows larger, high-reward unseen objects take up more total probability.**

This seems to be counter to our intuition on generalization; which suggests that as a model gets more training data, it should extrapolate better (which for a probability model should mean that $p(x; \theta)$ should get closer to $p(x)$).

This result seems to be both terrible news and great news. First the bad news; this result suggests that naively applying GFN objectives to an offline training regime simply doesn’t work. Indeed, intuitively because Z is a free variable in GFNs, one of two things seems likely to happen: either the model ends up learning $Z = \sum_{i \in \text{train}} R(x_i)$ and giving 0 probability to the test set, or the model ends up learning an arbitrary large Z and giving 0 probability to the training set. The good news; while the latter seems to happen (the training set ends up with fairly low total probability), there seems to be *structure* to which states receive the most probability. This again seems particularly useful in the scenario where we are looking for the most interesting (high-reward) x .

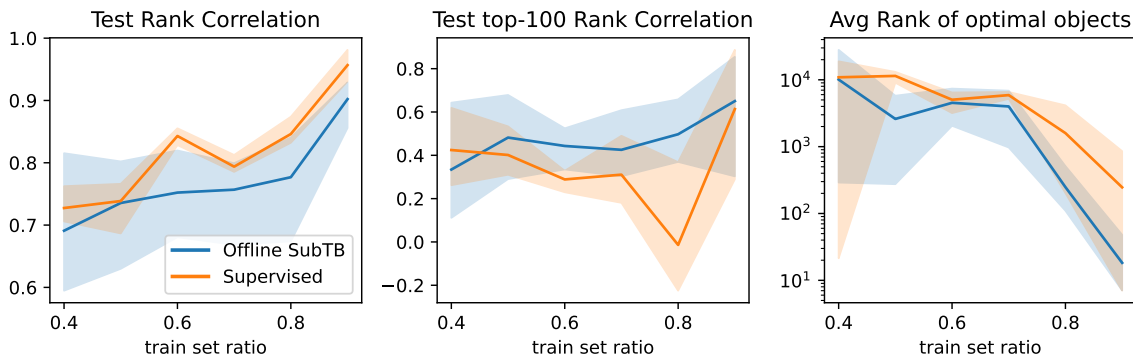


Figure 19. Rank-related metrics during offline GFN training and supervised regression as a function of the size of the training set. Averages are over 4 seeds (which influence the construction of the test).

E. Sequence and Hypergrid Experiments

E.1. Online and distilled training

E.1.1. ONLINE TRAINED MODELS

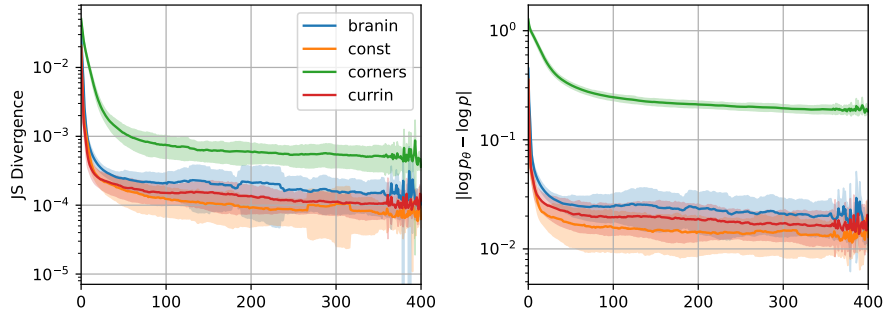


Figure 20. Training a GFlowNet (online and on-policy) on 4 different **hypergrid** tasks. Corners, the most frequently used task in the hypergrid environment, appears to be most difficult for learning $p(x)$.

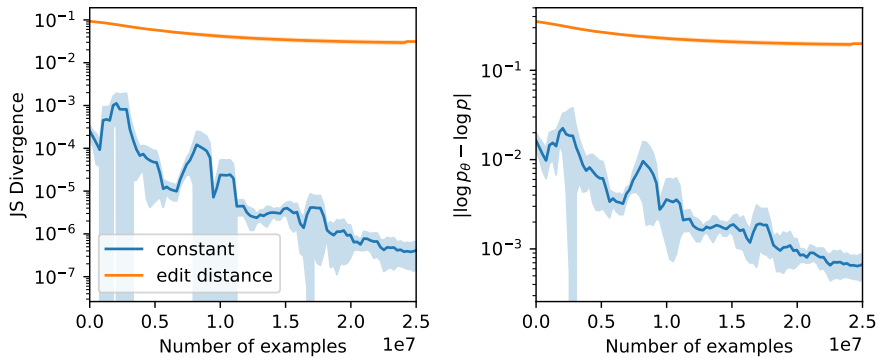


Figure 21. Training a GFlowNet (online and on-policy) on 2 different **sequence** tasks. The edit distance task appears to be significantly more difficult than the constant task for learning $p(x)$. Given the auto-regressive nature of the sequence environment, it is not surprising how well a GFlowNet performs on the constant task (i.e. the sequence environment is not challenging on its own). In contrast, we reify that the edit distance reward is indeed a challenging task in this environment.

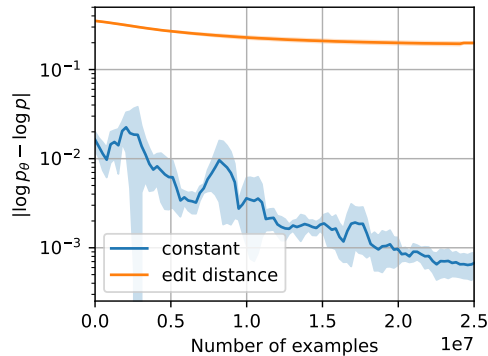


Figure 22. MAE error for only test states on the sequence task for online and on-policy. Note that for this experiment, the test states are not necessarily unvisited by the model

E.1.2. DISTILLED FLOWS AND FORWARD POLICY MODELS

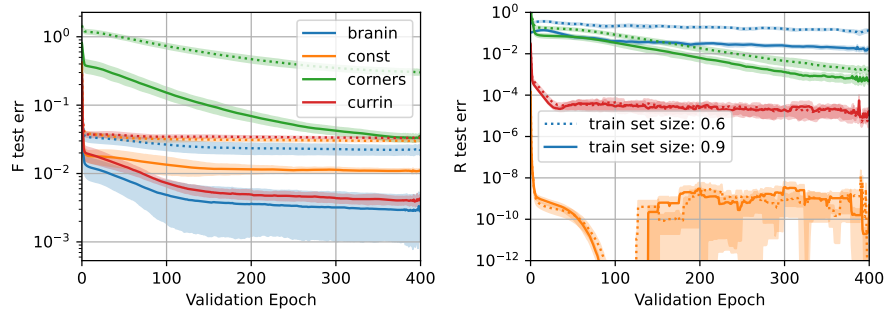


Figure 23. Training a MLP on 4 different tasks to regress to F (left) and R (right) in the **hypergrid** environment. Task difficulty between supervised models and online and on-policy trained GFlowNets appears consistent.

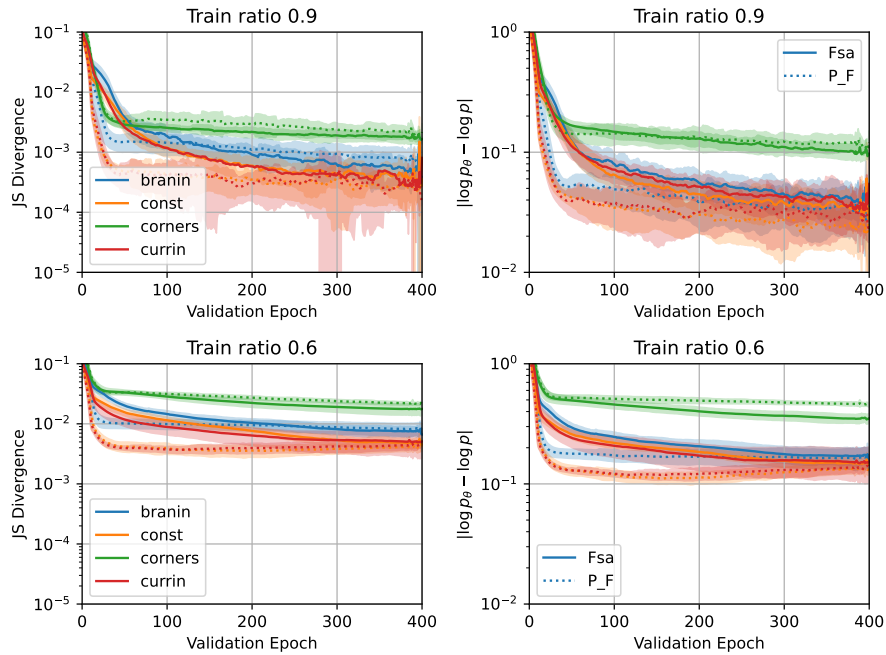


Figure 24. Training a model to distill edge flows and policies on 4 different **hypergrid** tasks for 90%-10% train-test split (top) and 60%-40% train-test split (bottom). It generally seems that (a) doing so recovers the intended distribution fairly well, and (b) modeling P_F appears easier than modeling F , insofar as it recovers $p(x)$ better, in the hypergrid environment.

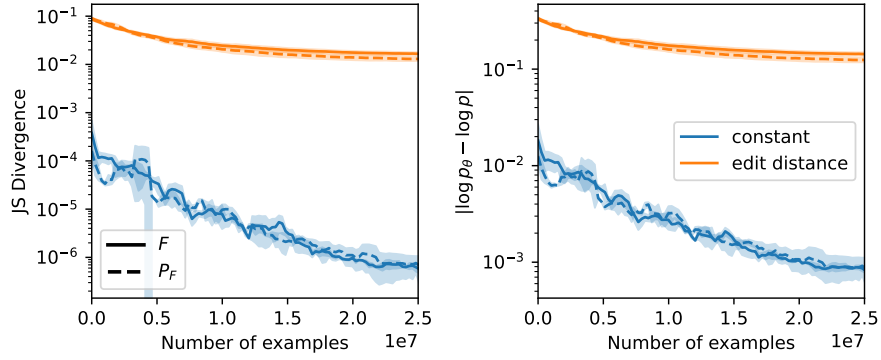


Figure 25. Training a model to distill edge flows and policies on 2 different **sequence** tasks for 90%-10% train-test split. It generally seems that (a) doing so recovers the intended distribution fairly well, and (b) modeling P_F appears easier than modeling F , insofar as it recovers $p(x)$ better, in the sequence environment for the edit distance reward. For the constant reward, there appears to be no apparent difference in difficulty between learning P_F or F .

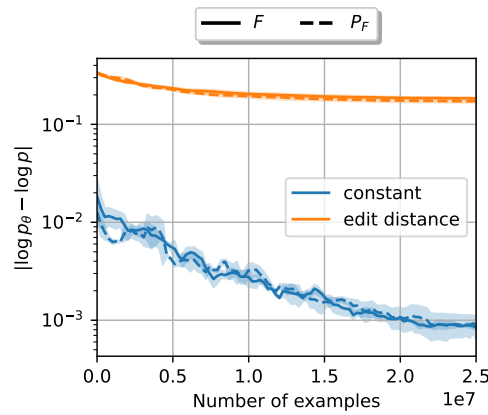


Figure 26. MAE error for only test states on the **sequence** task for distilled model, regressed to P_F . Note that for this experiment, the test states are unvisited by the model.

E.2. Reward transformation

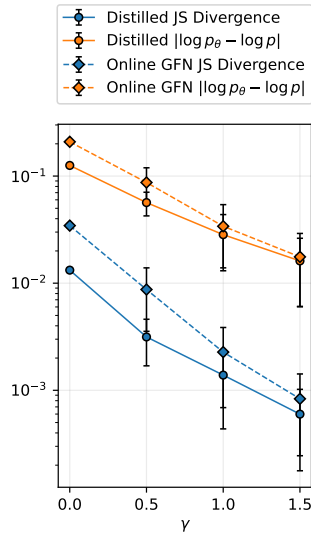


Figure 27. Training models distilled to P_F and GFlowNet models trained online/on-policy for a range of monotonic skew values γ on the **sequence** task. Transforming the distribution of the edit distance reward to contain a larger proportion of high reward values generally improves the performance for approximating $p(x)$.

E.3. Memorization gap experiments

E.3.1. MEMORIZATION IN HYPERGRIDS

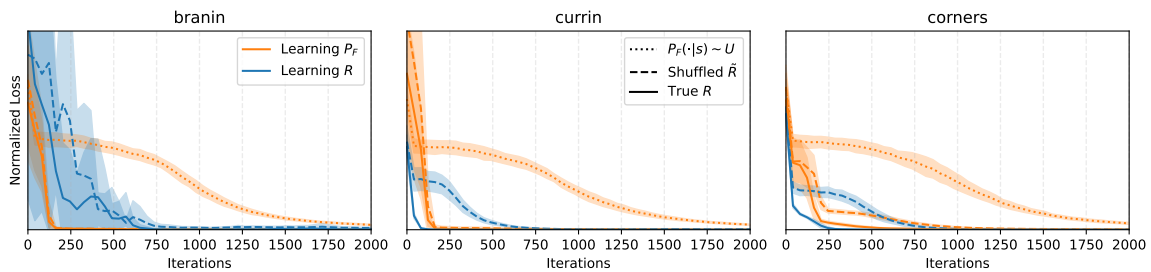


Figure 28. Memorization gap training curves for branin, currin, and corners tasks on the **hypergrid** environment. Maintaining *flow* structure in the learning problem (learning P_F under shuffled \tilde{R}) generally induces a smaller *memorization gap* relative to the fully de-structured setting. Note that for the branin reward, there is not apparent difference between learning the true R and the shuffled \tilde{R} , suggesting the reward alongside the hypergrid environment induces a task with minimal difficulty.

E.3.2. MEMORIZATION IN SEQUENCES

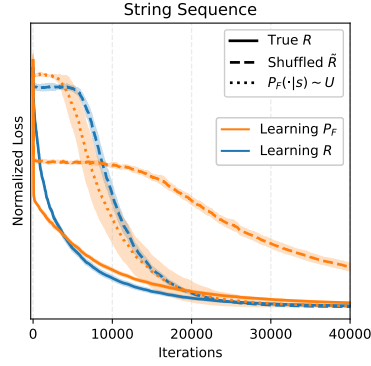


Figure 29. Memorization gap training curves for the edit distance task on the **sequence** environment. Maintaining *flow* structure in the learning problem (learning P_F under shuffled \tilde{R}) generally induces a smaller *memorization gap* relative to the fully de-structured setting.

E.4. Offline and off-policy training

E.4.1. OFFLINE AND OFF-POLICY IN HYPERGRIDS

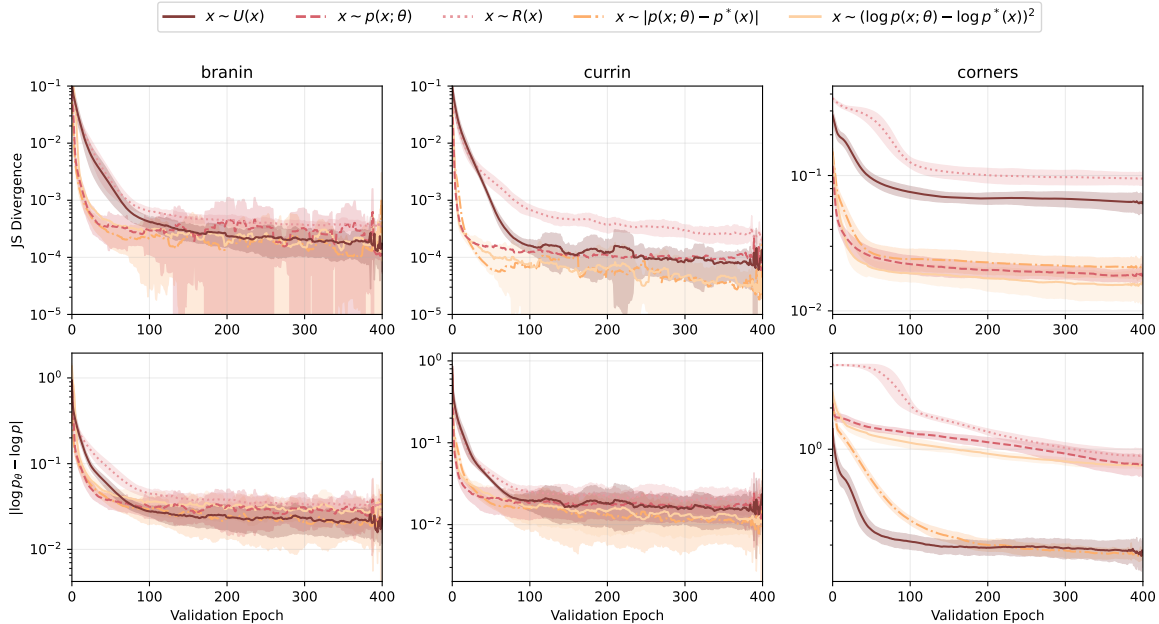


Figure 30. Evaluation curves for offline and off-policy trained GFlowNets on branin, currin, and corners **hypergrid** tasks for different choices of $\mathbb{P}_{\mathcal{X}}$ when training using a subset of the full dataset (90%-10% train-test split). In this setting, agnostic to the choice of $\mathbb{P}_{\mathcal{X}}$ and hypergrid reward, we observe the GFlowNet models converge when considering both the JS divergence and the MAE distributional metrics for approximating $p(x)$. This differs from the graph generation tasks where models struggle to converge on these metrics in this setting. For the more difficult task (corners), sampling x from sets that include the proxy-policy $p(x; \theta)$ result in the best performance on JS divergence while sampling $x \sim \mathcal{U}$ and $x \sim |\log p(x; \theta) - \log p(x)|$ results in the best performance on the MAE metric.

E.4.2. OFFLINE AND OFF-POLICY IN SEQUENCES

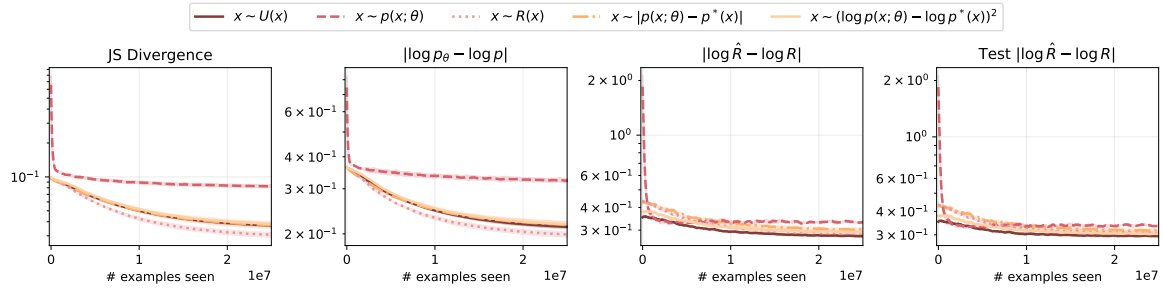


Figure 31. Evaluation curves for offline and off-policy trained GFlowNets on edit distance **sequence** task for different choices of $\mathbb{P}_{\mathcal{X}}$ when training using a subset of the full dataset (90%-10% train-test split). In this setting, agnostic to the choice of $\mathbb{P}_{\mathcal{X}}$, we observe the GFlowNet models converge when considering JS divergence and MAE distributional metrics for approximating $p(x)$. This differs from the graph generation tasks where models struggle to converge on these metrics in this setting.